ELSEVIER

Tectonophysics 296 (1998) 15–29

TECTONOPHYSICS

Stability and growth of continental shields in mantle convection models including recurrent melt production

J.H. de Smet *, A.P. van den Berg, N.J. Vlaar

Department of Theoretical Geophysics, University of Utrecht, P.O. Box 80.021, 3508 TA Utrecht, Netherlands

Accepted 5 February 1998

Abstract

The long-term growth and stability of compositionally layered continental upper mantle has been investigated by numerical modelling. We present the first numerical model of a convecting mantle including differentiation through partial melting resulting in a stable compositionally layered continental upper mantle structure. This structure includes a continental root extending to a depth of about 200 km. The model covers the upper mantle including the crust and incorporates physical features important for the study of the continental upper mantle during secular cooling of the Earth since the Archaean. Among these features are: a partial melt generation mechanism allowing consistent recurrent melting, time-dependent non-uniform radiogenic heat production, and a temperature- and pressure-dependent rheology. The numerical results reveal a long-term growth mechanism of the continental compositional root. This mechanism operates through episodical injection of small diapiric upwellings from the deep layer of undepleted mantle into the continental root which consists of compositionally distinct depleted mantle material. Our modelling results show the layered continental structure to remain stable during at least 1.5 Ga. After this period mantle differentiation through partial melting ceases due to the prolonged secular cooling and small-scale instabilities set in through continental delamination. This stable period of 1.5 Ga is related to a number of limitations in our model. By improving on these limitations in the future this stable period will be extended to more realistic values.

Keywords: numerical model; continental root; depletion; Archaean; evolution; stability

1. Introduction

Several geodynamical scenarios exist which address the continental formation during the early evolution of the Earth (Jordan, 1988; Anderson, 1990; Vlaar et al., 1994). The stability of the continental root, differences between oceanic and continental lithosphere, the thickness of the continental lithosphere, and differences between old cratonic and younger continental lithosphere are some of the issues addressed by such geodynamical scenarios. Evidence for a specific continental configuration extending over several hundreds of kilometres in depth comes from different disciplines.

Based on seismological observations, Jordan (1975) finds that the present-day lithosphere of old continental nuclei must be significantly cooler than recent oceanic lithosphere. This led him to the concept of the continental 'tectosphere'. An overview and discussion of evidence supporting the existence of the tectosphere is given by Jordan (1988) where it

* Corresponding author. Fax: +31 (30) 253-5030; E-mail: smet@geof.uu.nl

0040-1951/98/$19.00
PII: S0040-1951(98)00135-8

is argued that it extends to 250–400 km depth, depending on its age of formation. Other studies which discuss seismological observations concerning the structure of continental lithosphere (Anderson, 1990; Polet and Anderson, 1995) are in agreement with this observation, although the estimates of the depth extent of the cratonic root are smaller. Similar conclusions were drawn by Doin et al. (1996) on the basis of geoid inversions.

The concept of the continental tectosphere explains the long-term stability of ancient (>3 Ga) continental shield areas by compositional layering. In this model a layer of depleted mantle peridotite of lower intrinsic density lies on top of a layer of undepleted denser peridotite (Jordan, 1978, 1988). Depleted peridotite is the residual material in the mantle differentiation process of pressure release partial melting, resulting in production and segregation of basaltic melt.

Geodynamical consequences for the evolution of the Earth of this differentiation process in an oceanic setting were investigated by Vlaar and van den Berg (1991), using a modification of the model by McKenzie (1984) for 1-D pressure release melting. Vlaar et al. (1994) used a more extended model to investigate the role of the upper mantle differentiation process in the Earth's secular cooling. Particularly in Vlaar and van den Berg (1991) and Vlaar et al. (1994) it was demonstrated that in the early Earth when partial melting takes place at higher mantle temperature, a much thicker basaltic crust and corresponding thicker depleted peridotite layer are produced. This creates an intrinsically stable layering and conditions which do not favour a present-day style of plate tectonics. In the present paper an extended formulation for partial melting not restricted to 1-D adiabatic conditions is applied to investigate how Archaean continental shields have evolved. We assume a higher mantle temperature consistent with secular cooling of the Earth since the early Archaean. This paper is focused on some of the major topics concerning the evolution of old continental shield. Among these are the stability, growth and cooling behaviour of the continental mantle. To this end we have used a numerical model for thermo-chemical mantle convection that includes mantle differentiation by means of partial melting. Our model is the first one exhibiting a convecting mantle with partial melting that produces a stable layering of lighter depleted peridotite on top of a fertile peridotite layer.

Alternative convection models have been applied to the upper mantle by different authors. Ogawa (1988, 1993, 1994) focuses on upper mantle differentiation in the context of the Earth's evolution. The model of Doin et al. (1997) includes an ad hoc continental region of which the stability is studied. The model of Lenardic (1997) is appropriate to study the variation of continental heat flow variations. Upper mantle differentiation in mantle convection has also been studied by Schmeling and Bussod (1996) for present-day continental conditions.

The next section discusses the numerical model. The model incorporates important physical aspects which are necessary to study evolution of old continental lithosphere. This includes recurrent melting of partially depleted material, which is important to study possible growth mechanisms of the depleted continental root in a convecting mantle. According to Jordan (1988) two growth mechanisms can be responsible. The first is a process of steady internal depletion of the continental root. The second one adds depleted material from below. Which one of these, or possibly other mechanisms cause the growth remains an unanswered question. At least one such mechanisms, however, is required to stabilize the continental lithosphere during secular cooling. The modelling results presented illustrate clearly the different possibilities of active growth mechanisms and their relative importance. The model presented here includes the physics that covers both growth mechanisms, and from the modelling results their relative importance can be investigated. Thermal aspects are also discussed in this work, since they influence the stability of the tectosphere. To this end, several important thermal effects are incorporated: cooling due to adiabatic decompression, internal radiogenic heating, and directly connected to the melting process, the effect of latent heat consumption.

The combination of the consistent partial melting with the aforementioned thermal aspects, and a parameterization that is thought to be applicable to an Archaean continental situation results in a model that can explain how continental roots have grown during the Earth's secular cooling and why they have remained stable in the process.

2. Model description and numerical method

The state of differentiation of the mantle is described by the degree of depletion expressed as the mass fraction F of the produced partial melt: $0 \leq F < 1$. A zero value of the degree of depletion corresponds to a pyrolite primitive upper mantle and a gradually increasing F corresponds to low degrees of partial melting resulting in a lherzolitic residue, and for even larger values of F the residue is harzburgitic (Ringwood, 1982). This compositional effect (Jordan, 1979) is translated into a density effect which influences the gravitational stability of the system as shown by Vlaar and van den Berg (1991) and Vlaar et al. (1994). Including the effect of thermal expansion the linearized equation of state is:

$$\rho(T, F) = \rho_0 \left[1 - \alpha(T - T_{\text{srf}}) - F\delta\rho/\rho_0\right] \quad (1)$$

Symbols are defined in Table 1 and all quantities in Eq. 1 are in dimensional form. We used a non-dimensionalization scheme described in Van den Berg et al. (1993). In the following equations non-dimensional quantities are used unless explicitly stated otherwise. The equation of state defines the buoyancy force in the non-dimensional momentum equation through the thermal and compositional Rayleigh numbers *Ra* and *Rb*, respectively. For an infinite Prandtl number fluid this yields:

$$\nabla \cdot \left[\eta(\nabla \boldsymbol{u} + \nabla \boldsymbol{u}^T)\right] - \nabla \Delta p = (RaT + RbF)\hat{z} \quad (2)$$

where $\hat{z}$ is the unit vector in the vertical direction aligned with gravity. The definitions of $\boldsymbol{u}$, Δp, *Ra* and *Rb*, and the values *Ra* and *Rb* are listed in Table 1.

We assume a Newtonian pressure- and temperature-dependent viscosity defined by an Arrhenius relation:

$$\eta(p, T) = \mathcal{B}(F) \cdot \exp\left(\frac{E + pV}{RT}\right) \quad (3)$$

where the temperature, pressure and viscosity are in dimensional form. The numerical values of the activation parameters E and V for dry olivine are taken from Ranalli (1991) and Karato and Wu (1993) and listed in Table 1. The pre-factor $\mathcal{B}$ contains the dependence on the degree of depletion F (see below) and is chosen such that at 400 km depth, 1750°C and $F = 0$ the viscosity equals the reference viscosity $\eta = \eta_0 = 10^{21}$ Pa s. The top part of the model is a mechanical boundary layer (MBL) with a high-viscosity lid. For numerical reasons we truncated the viscosity distribution near the cold top boundary at $\eta_{\max} = 10^{24}$ Pa s. The average mantle geotherm in the model results in a layer of minimum viscosity directly underneath this MBL. Such a rheological layering is also found in viscosity profiles derived from post-glacial rebound analysis (Lambeck et al., 1996). The stabilizing effect of the MBL is enhanced by the buoyant crustal layer of lower density ρ_c. Internal heating by radioactive decay is strongest in the crustal part, resulting in a thermal blanketing effect and slower cooling. The buoyant MBL prevents the gravitational collapse of the upper continental lithospheric part of the model during secular cooling. At greater depths the pressure dependence dominates over the temperature effect and hence the viscosity increases. This makes the deeper part of the upper mantle less mobile, restricting the mantle circulation to shallower depths in our model. We have investigated two different rheological models. In one model we assume the viscosity of the residual material to be larger than for undepleted rock, i.e. $\mathcal{B}(F) = 5 \cdot \mathcal{B}(0)$ when $F > 0$ in Eq. 3. The model with F-dependent rheology is referred to as Model B and the model with uniform $\mathcal{B} = \mathcal{B}(0)$ is referred to as Model A.

We assume a simplified parameterization of the melting phase diagram with linear and parallel solidus and liquidus between which F is a bilinear function of p and T based on experimental data compiled by Jacques and Green (1980). The transport equation describing partial melting of a volume of mantle material in terms of the degree of depletion F is:

$$\frac{\mathrm{d}F(p, T)}{\mathrm{d}t} = \frac{\mathrm{d}f(\Theta)}{\mathrm{d}t} \quad (4)$$

where the right-hand-side describes a source distribution of partial melt production and Θ is a normalized super-solidus temperature further defined in Appendix A. A volume of partially melted material that is being recycled can only differentiate further when its Θ value is in excess of any previously reached value.

The energy equation based on the Extended Boussinesq Approximation (EBA) (Ita and King, 1994) is written in non-dimensional form using the

Table 1
Notations

Symbol	Definition	Value	Units
α	thermal expansion coefficient	3×10^5	K^{-1}
ρ_0	reference density	3416	kg m^{-3}
ρ	effective density $\rho(T, F)$	–	kg m^{-3}
ρ_c	crustal density at $T = T_{srf}$	3000	kg m^{-3}
$\delta\rho$	density drop upon full differentiation	226	kg m^{-3}
η	non-dimensional viscosity	–	–
η_0	reference viscosity	10^{21}	Pa s
η_{max}	maximum viscosity	10^{24}	Pa s
E	activation energy	250	kJ mol^{-1}
V	activation volume	7.5	μm^3 mol^{-1}
R	gas constant	8.3143	J mol^{-1} K^{-1}
$\mathcal{B}$	viscosity pre-factor	9×10^{11}	Pa s
F	degree of depletion or mass fraction of the melt	–	–
$\boldsymbol{u}$	velocity	–	m s^{-1}
T	non-dimensional temperature	–	–
$\langle T\rangle$hor	horizontally averaged temperature	–	–
ΔT	temperature scale	2200	K
T_{srf}	surface temperature	273.15	K
T_0	non-dimensional surface temperature $T_{srf}/\Delta T$	0.12416	–
$T_s(p)$	pressure-dependent solidus temperature	–	K
$T_l(p)$	pressure-dependent liquidus temperature	–	K
$T_s(p = 0)$	solidus temperature at zero pressure	1115	ºC
p	pressure	–	Pa
Δp	non-dimensional hydrodynamic pressure	–	–
h	depth scale	670	km
λ	radioactive decay constant	0.347	$(Ga)^{-1}$
κ	thermal diffusivity	10^{-6}	m^2 s^{-1}
k	thermal conductivity	3.416	W m^{-1} K^{-1}
c_p	heat capacity at constant pressure	1000	J kg^{-1} K^{-1}
dT_s/dp	slope of solidus and liquidus	120×10^{-9}	K Pa^{-1}
ΔT_{sl}	distance between solidus and liquidus	600	K
ΔS	entropy change upon melting	300	J kg^{-1} K^{-1}
H	non-dimensional radiogenic heat generation	–	–
H_0	reference value radiogenic heat generation	5.33×10^{-6}	W m^{-3}
$\mathcal{R}$	internal heating number $H_0 \cdot (h^2)/(k\Delta T)$	318.4	–
Di	dissipation number: $(\alpha g h)/(c_p)$	0.1970	–
Rb	compositional Rayleigh number: $(\delta\rho g h^3)/(\kappa\eta_0)$	0.6661×10^6	–
Ra	thermal Rayleigh number: $(\rho_0\alpha\Delta T g h^3)/(\kappa\eta_0)$	0.6645×10^6	–

non-dimensionalization scheme described in Van den Berg et al. (1993):

$$\frac{dT}{dt} - Di(T + T_0)u_z = \nabla^2 T + \mathcal{R}H(\boldsymbol{x}, t) - (T + T_0)\frac{\Delta S}{c_p}\frac{dF}{dt} \qquad (5)$$

where the viscous dissipation term is neglected and Di is the dissipation number defined in Table 1. Latent heat consumption by partial melting is represented by the last term. The term containing the dissipation number Di accounts for heating and cooling due to adiabatic (de-)compression. Taking this effect into account is essential in stability experiments. This is reflected in the fact that the critical Rayleigh number for Rayleigh–Benard convection is higher (Steinbach, 1991) compared to the Boussinesq case with $Di = 0$.

We have used a non-uniform distribution of internal heat production with the maximum values in the crustal layer. Increased internal heating in the top layers results in a strong blanketing effect which in

turn delays the cooling from the top. This increases the stability of the layering significantly.

The present-day continental situation of the heat production in the 16 km thick upper crust initially follows $H(\boldsymbol{x}, 0) = H_0 \cdot \exp(-z/b)$ with $b = 30$ km and $H_0 = 2.67$ μW m^{-3}. In the lower crust up to 50 km depth a uniform $H_l = 0.45$ μW m^{-3}, and for undepleted mantle material a lower uniform productivity of $H_u = 0.045$ μW m^{-3} is valid. Total segregation of melt as assumed in our model will remove most of the incompatible radiogenic elements and the value of H for this case is assumed to drop to $H_d = 0.02$ μW m^{-3}. Radiogenic heating is essential to establish a realistic continental geotherm. The values given above for H represent the present-day situations of continental shields according to Chapman (1986). The upper crustal value is in agreement with O'Connell and Hager (1980). Estimations of H applicable to the Archaean era vary from two to three times the present-day value. We have applied the lower bound in our model. Multiplying all the above given figures by two yields $H_0 = 5.33$, $H_l = 0.9$, $H_u = 0.09$ and $H_d = 0.04$ μW m^{-3}. The choice of the value of 2 for the radioactive decay factor results in an underestimation of the Archaean radiogenic heat production.

Melt segregation due to mantle differentiation is the prime cause for the non-uniform heat production as described above. Since the influence of this process on separate radioactive isotopes is rather uncertain, and isotope concentrations are not precisely known for the Archaean era, multiplication of each layer separately by the same factor of 2 gives only an approximation of the Archaean distribution. Furthermore, there are many other uncertainties, such as the amount of erosion and the parameter b and the isotope-dependent radioactive decay constant λ, which also influence the validity of this extrapolation. The effective radioactive decay constant is set to $\lambda = 0.347$ Ga^{-1} (Turcotte and Schubert, 1982. When the melt is expelled, it is removed from the model and is not added to the crustal mass. This implicitly assumes that erosion balances the melt production and that the crustal heat generation is not affected by these processes.

The momentum and energy equations are solved with a finite element method (Van den Berg et al., 1993) and a time-dependent upwind scheme (SUPG) (Hughes and Brooks, 1979; Segal, 1982) is applied to the latter to improve numerical stability in advection-dominated regions of the domain. The transport equation for F is solved using a method of characteristics on a mesh much denser than the finite element mesh. A fourth-order Runge–Kutta integration scheme is applied in combination with a hybrid interpolation scheme. Bilinear interpolations (Sotin and Parmentier, 1989; Sparks and Parmentier, 1993) form one part of this hybrid scheme. The other part consists of bicubic spline interpolations (Ten et al., 1996). Eqs. 2, 4 and 5 are solved in this order.

3. Numerical modelling results

We present modelling results for a rectangular domain with a depth of 670 km and an aspect ratio $a = 3$ corresponding to a width of 2010 km. The bottom boundary represents the interface between the upper and lower mantle. A zero heat flux condition is applied to the bottom boundary, resulting in an overestimated cooling rate for the model. The vertical boundaries are thermally isolated and the top of the crust has a fixed surface temperature T_{srf}. All boundaries are impermeable and a free slip condition is imposed on them. The two rheologically different models mentioned in the previous section have been investigated.

3.1. Initial condition

The purpose of our modelling experiments is to investigate the growth and the long-term evolution of a differentiated, layered continental upper mantle. Since the actual upper mantle conditions in the early Earth are largely unknown, we have constructed a dynamical initial condition for the time-dependent model calculations.

The dynamical initial condition is created in the following way: the model Eqs. 2 and 5 are integrated in time for a duration of several hundred million years for an undifferentiated mantle. In this start-up run, partial melting is switched off and radiogenic heating is defined constant in time and purely depth-dependent, i.e. $H = H(z)$. During this initial convection stage, a thermal state of the mantle develops which is determined fully by the distribu-

tion of heat sources and the boundary conditions. As a result a statistically stationary situation evolves with $F = 0$ throughout the model. When this situation is reached, mantle differentiation in the model is switched on and the thermo-chemical evolution starts. Radioactive decay is also started at this moment, which we will refer to as $t = 0$ Ma.

As will be shown below, mantle differentiation starts rapidly after $t = 0$ Ma and after only a few million years a gravitationally stable, partially depleted layer has developed directly below the crust. This depleted layer then evolves with a much lower growth rate, driven by the secular cooling of the upper mantle. This observation suggests that transient effects due to the dynamical initial condition are limited in time to about 10 Ma. The evolution of the layered system which is relevant in the present context starts after this initial phase.

The initial crustal thickness of 50 km does not change during the computations since crustal accumulation of melt is not implemented in the model. The crustal layer is part of the MBL and as such it is allowed to deform mechanically under the influence of viscous stress resulting from the mantle convection currents. The crust has an important stabilizing effect on the layering of the uppermost mantle during the start-up run and after. The high internal heating of the crust results in a strong thermal blanketing effect. Furthermore, its low density and high viscosity prevent the relative cold boundary layer from gravitational collapse. Experiments with thinner crusts revealed the same configuration of a depleted mantle directly under this crustal layer. The major effect of a thinner lower crust is a reduction of the crustal blanketing effect due to the reduced radiogenic heat production in the lower crust. This would result in a slightly cooler geotherm and in a reduction of the thickness of the depleted zone. However, this reduction of the thickness of the depleted zone is counteracted by the fact that the top of the depleted zone would be at a shallower depth. A more detailed description of processes which influence the crustal thickness such as erosion and melt accumulation are not included in our model. However, for reasons described above we expect the crustal thickness in the model to have a minor influence on the model evolution.

3.2. Global thermo-chemical evolution

An impression of how the mantle model evolves compositionally and thermally is given in Fig. 1 for Model A. The depletion field F (left-hand column) and the modified temperature field $T - \langle T \rangle_{\mathrm{hor}}$ (right-hand column), which is used to emphasize the small lateral variations in the temperature field with respect to the 1-D background temperature, are shown for three different time values. Contours of the stream function Ψ are also plotted. Black and white contours are used for positive and negative values of Ψ to distinguish the orientation of the flow field. The streamlines show a large-scale sluggish convection pattern below the zone of the depleted layer and a small-scale convection pattern decaying in time in the continental root. The small-scale thermo-chemical convection pattern in the rapidly developing continental root during the initial formation phase is related to the dynamic initial condition discussed above. Fig. 1a1,b1 shows that the vigour of convection throughout the upper mantle is strongly decreased after 71 Ma and that the bulk of the continental root already has developed. The low-density root limits large-scale convection to the mantle underneath it.

Due to the mechanical boundary conditions, blobs of cold depleted material flow down at the vertical boundaries of the domain illustrated at the right-hand boundary in Fig. 1b1,b2. This descending depleted material is absorbed in the deeper mantle as shown in the last pair of frames at almost 1 Ga (Fig. 1c). This artifact due to boundary conditions contaminates the development of the whole system, especially when aspect ratios smaller than 2 are used. The net effect of this contamination of the deep upper mantle is that the effective density contrast between continental root and underlying mantle decreases, thereby also decreasing the gravitational stability of the layering in the presented model.

The temperature fields depicted in the right-hand column of Fig. 1 illustrate that cooling from the top slowly penetrates into the lower mantle. Some correlation between temperature and depletion F can be observed, for instance in cold blobs, slightly depleted, descending from the bottom of the depleted zone. This is most clearly depicted in Fig. 1b. An overall characteristic of Fig. 1 is that of rapid growth

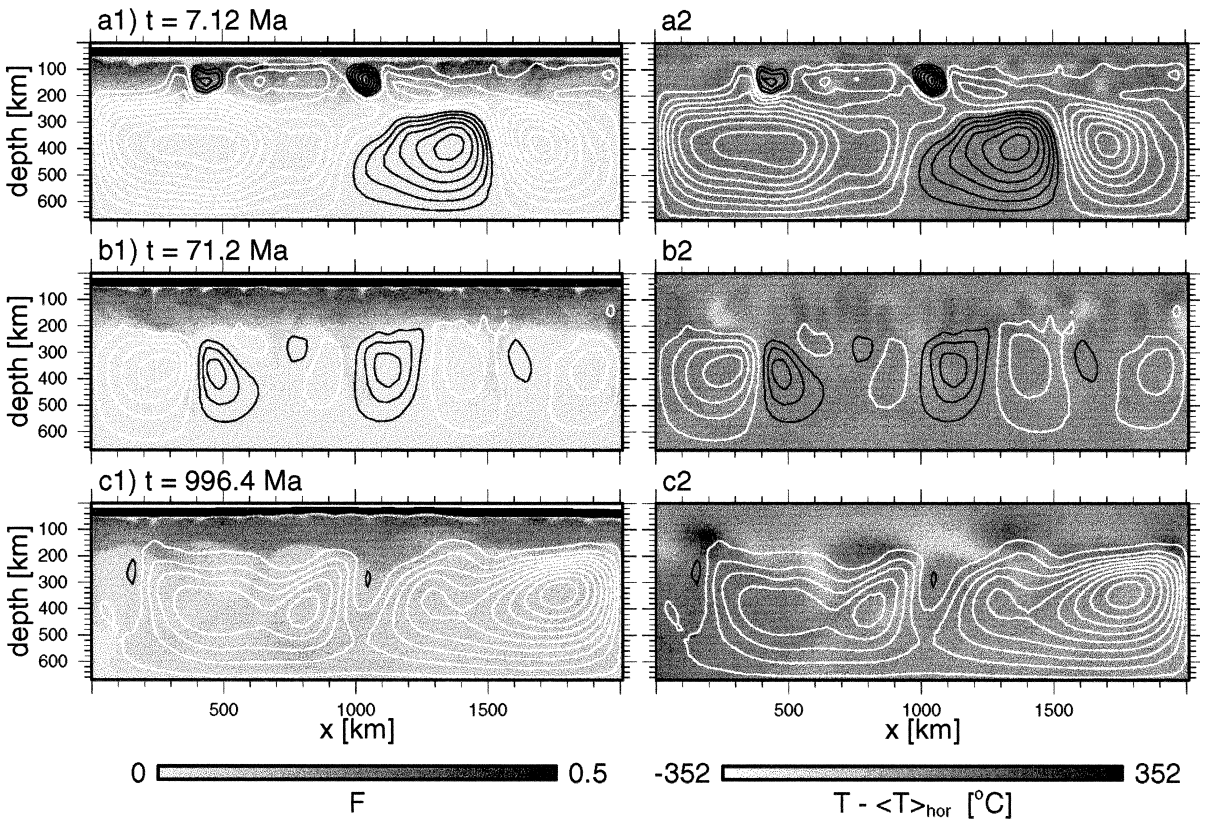

Fig. 1. Contour plots of F (a1–c1), $T - \langle T \rangle_{\mathrm{hor}}$ (a2–c2) and streamlines during the spin-up phase (a), after 71.2 Ma evolution time (b), and after almost 1 Ga evolution (c). The white and black streamlines in all depictions indicate clockwise and counterclockwise flows, respectively. In a1–c1 the thin white layer on top is the upper crust and the lower crust is coloured as a black layer underneath it. The harzburgite layer denoted dark grey is formed during a short period of time, and it continues to grow at a much slower rate. Cooling from the top penetrates through the continental root (a2–c2) creating a 200 km thick MBL.

of the continental root situated in the upper 200 km of the mantle.

3.3. Quantification of the global evolution

In Fig. 2 time series of several global quantities are shown. The time series begin with the start-up period of 300 Ma preceding $t = 0$ Ma during which the aforementioned dynamic initial condition evolves. This formation of a statistically stationary situation is clearly illustrated in the volume average temperature shown in Fig. 2b. This curve shows that the model reaches a statistically thermal equilibrium approximately 150 Ma before mantle differentiation is started at $t = 0$ Ma. Similarly the time series of the root mean square velocity (V_{rms}) shown in Fig. 2a fluctuates about a stationary state.

At $t = 0$ Ma mantle differentiation through partial melting is switched on in the model. As a result upwelling flows of low-density depleted material develop rapidly starting the growth of the depleted zone below the crust. These ascending and differentiating upwellings are accelerated in their upward motion due to the fact that the compositional buoyancy dominates the counteracting effect of cooling by latent heat consumption and adiabatic decompression. The spin-up in V_{rms} shown in Fig. 2 during this initial stage lasts approximately 10 Ma. After the initial spin-up stage a layered system has evolved which represents a young Archaean configuration in our model.

Fig. 2a shows the strong effect of the density layering created during the spin-up stage on the convection dynamics. The vigour of convection is

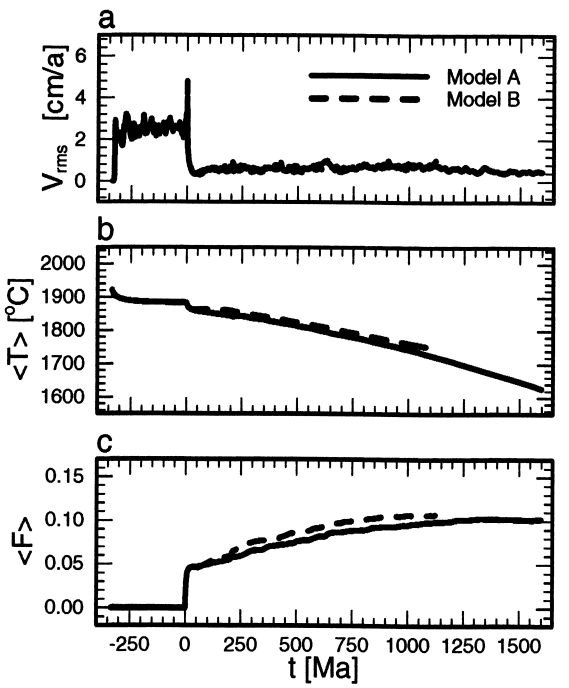

Fig. 2. Time series of volume-averaged quantities for Models A (solid lines) and B (dashed lines). (a) The root-mean-squared velocity. (b) The volume-averaged temperature. (c) The volume-averaged degree of depletion. During the first 300 Ma shown ($t < 0$ Ma) the statistically stationary dynamical initial condition evolves. At $t = 0$ Ma mantle differentiation is allowed to start in the model resulting in a transient spin-up phase with a duration of almost 10 Ma.

strongly reduced as a result of the increased internal stability of the layered system. The V_{rms} drops from a time averaged value of $\sim$2 cm/a just before the start of the spin-up at $t = 0$ Ma to $V_{\mathrm{rms}} \approx 0.4$ cm/a afterwards. The volume-averaged temperature $\langle T \rangle$ in Fig. 2b shows a small but sharp decrease at $t = 0$ Ma due to the consumption of latent heat during the spin-up phase. After the spin-up phase a gradual decrease of the upper mantle temperature occurs of approximately 250 K during the 1.5 Ga time window.

No dramatic events occur during the evolution of the system as shown by the quantities depicted in Fig. 2. Catastrophical root collapses would cause other spin-ups probably accompanied by massive melting. The continental root remains stable during the observed time-span.

The volume average degree of depletion $\langle F \rangle$ shown in Fig. 2c is slowly increasing after the initial spin-up. Fig. 2c shows a steep increase of $\langle F \rangle$ during the spin-up phase (i.e. up to $t \approx 10$ Ma) when the continental root is formed. Within this period there is a rapid increase in volume of depleted material positioned just below the crust as is depicted in Fig. 1a1.

From the different traces in Fig. 2 it can be concluded that the transient effect of the dynamic initial condition decays rapidly in approximately 10 Ma. After this initial start-up phase a stable growth of the layered continental upper mantle system continues throughout the observed time-span.

3.4. Layering and stability

Fig. 3 shows the depth distribution of several horizontally averaged quantities and vertical cross-sections at different time values. Averaged geotherms are shown in Fig. 3a, together with the solidus and liquidus used in our model. The initial temperature distribution appears to be above the solidus temperature in the depth range between the bottom of the crustal layer and 200 km depth. At later time values this depth range decreases and after about 100 Ma the average geotherm is completely below the solidus. From about $t = 100$ Ma on, melting only occurs in regions with a positive temperature deviation from the horizontally averaged background geotherm, such as hot upwelling diapirs.

Fig. 3b shows horizontally averaged viscosity profiles for the same time values. The location of minimum viscosity shifts to greater depths as secular cooling proceeds, illustrating the growth of the MBL which is an important factor in stabilizing the cold top boundary layer. The horizontally averaged root mean square velocity $\langle V_{\mathrm{rms}} \rangle$ is displayed in Fig. 3c. Below the strong lid of the high-viscosity crust the $\langle V_{\mathrm{rms}} \rangle$ increases rapidly in the low-viscosity region at $t = 0$ Ma. The velocity in this region decreases rapidly after $t = 0$ Ma both because of the increase in viscosity due to cooling from the top and also because of the rapid formation of the low-density depleted layer. At larger time values the location of maximum $\langle V_{\mathrm{rms}} \rangle$ shifts downward with the location of minimum viscosity.

Fig. 3d shows the horizontally averaged effective density distribution $\langle \rho(T, F) \rangle$. After $t = 0$ Ma a strong density inversion develops due to the lighter

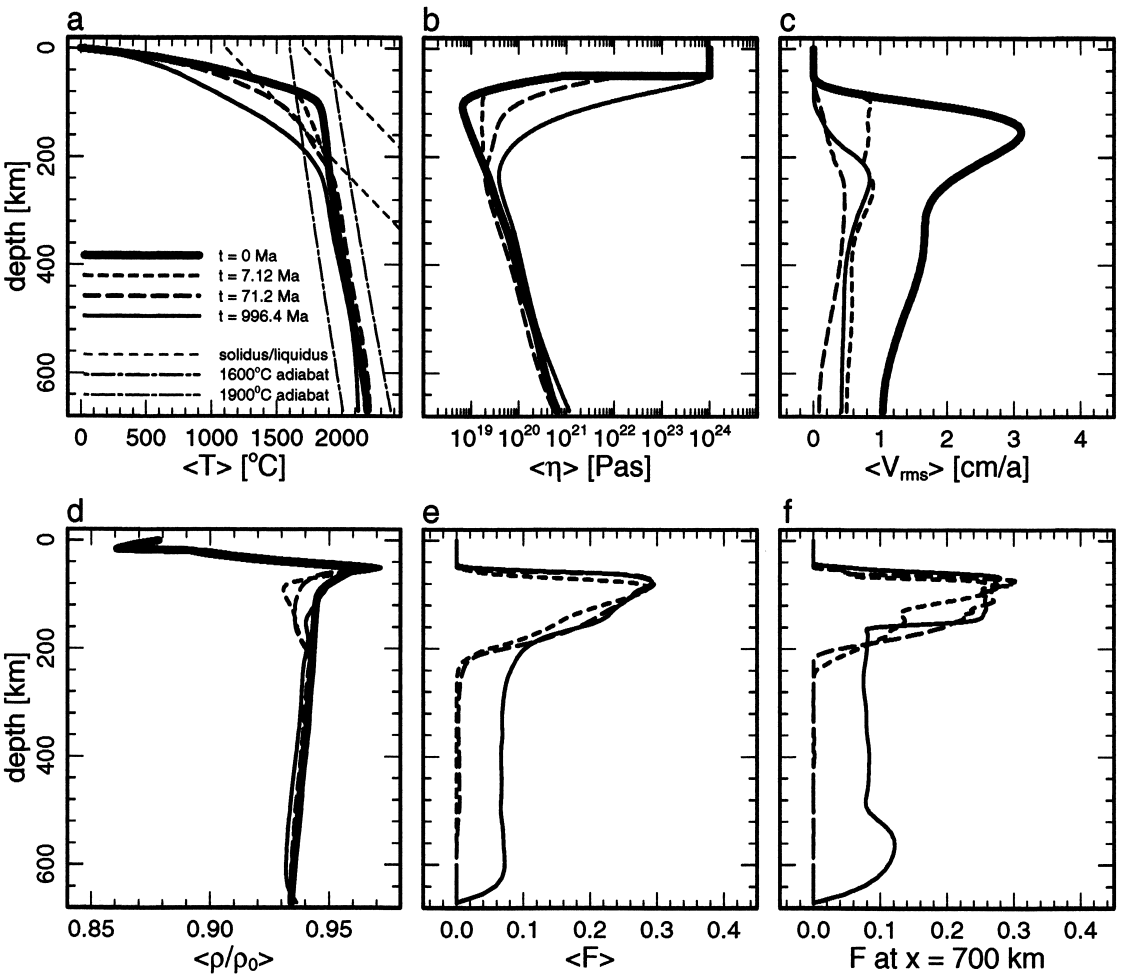

Fig. 3. Horizontally averaged profiles (a–e) and vertical cross-sections (f) for different time values for Model A. (a) Horizontally averaged geotherms. The dash–dotted lines are adiabats for the potential temperatures indicated. The dashed lines are the solidus (for $F = 0$) and liquidus lines. Surface heat flows are 150, 137 and 107 mW m^{-2} for $t = 7.12$ Ma, $t = 71.2$ Ma and $t = 996.4$ Ma, respectively. (b) Averaged viscosity profiles; note the slowly growing MBL. (c) Averaged V_{rms} profiles. (d) Averaged effective normalized density profiles clearly illustrating the density inversion in the continental root, decaying in time. (e) Averaged F. (f) Specific profile at given x; the profiles at $t = 0$ Ma are not shown for clarity.

depleted material accumulating at shallow depths. This density inversion is an important factor in the initial stabilization of the layering. For larger time values the density increases due to cooling from the top. High internal heating in the buoyant crust causes a thermal blanketing effect which slows down the cooling of the shallow layering. For later stages in the evolution the increase in viscosity shown in Fig. 3b prevents the collapse of the gravitationally unstable layering.

Horizontally averaged values of $\langle F \rangle$ and a vertical cross-section at $x = 700$ km of the degree of depletion are shown in Fig. 3f,g. These figures illustrate the rapid development of the depleted zone from $F = 0$ at $t = 0$ Ma to $t = 70$ Ma in the region between the crust to a depth of about 200 km. The finite values of F in the deeper part of the model at $t = 1$ Ga are related to the absorption of depleted material, originating from downwellings at the vertical boundary illustrated in Fig. 1. The detailed fine-scale layered structures in the depleted region shown in the profile of Fig. 3f are in part

remnants of the vigorous partial melting stage during the spin-up phase directly following $t = 0$. Some of the structures, however, are directly caused by the active ongoing growth process of the depleted zone. An illustration of this is given below.

3.5. The onset of instability, continental delamination

After approximately 1.5 Ga the character of the evolution changes. Gravitational instability due to cooling from the top is increasing. At the same time partial melting has stopped because upwelling flows in the convecting undepleted zone no longer cross the solidus due to the general temperature decrease illustrated by the 1 Ga geotherm in Fig. 3a. As the effective density contrast between the depleted zone and the layer beneath diminishes, large downwellings from the lower part of the depleted zone start to develop. Apparently the still growing MBL is no longer strong enough to prevent the increasingly unstable layering from collapse. However, these continental delaminations do not trigger any catastrophic events, such as upper mantle overturns, as is illustrated by the stationary character of the time series of the V_{rms} in Fig. 2. The delamination process cannot be studied in greater detail in our modelling results due to the lack of numerical resolution at greater depths. Because of this, numerical diffusion becomes too strong in the deeper regions, which induces that the downwellings are smoothly integrated in the deeper part of the upper mantle. Hence, higher grid resolutions must be used to study the phenomenon of delamination. The delamination of the deepest part of the depleted layer as observed in our model is a smaller-scale phenomenon than the one described by Pari and Peltier (1996).

3.6. Growth mechanism of the continental root

Fig. 4 shows the melt production rates integrated over the width of the domain (4a) and depth (4b), respectively, as a function of time. Fig. 4a shows that the depth range where partial melting occurs is between 110 and 240 km. The decrease in melt production amplitude shown in Fig. 4a is caused by the secular cooling of the mantle. Fig. 4a also shows that this decrease is accompanied by a narrowing of the

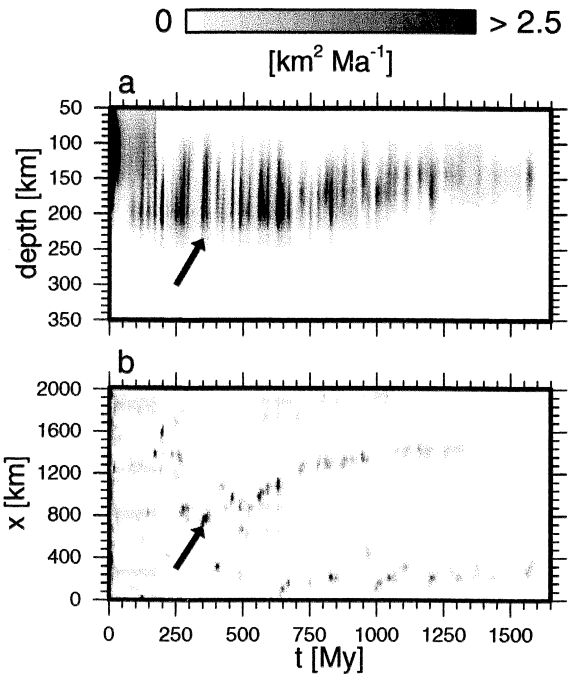

Fig. 4. 1-D depth (a) and horizontal (b) distribution of melt production for Model A as a function of time. The black arrows point to the partial melting event that is studied in more detail in Fig. 5.

depth range where melting occurs. The maximum depth where melting still occurs decreases when the mantle cools, which is in accordance with previous studies (Vlaar and van den Berg, 1991; Vlaar et al., 1994). Both Fig. 4a and Fig. 4b indicate that the melting process has a pulsating nature. Small localized events that last for no longer than 50 Ma which have a lateral extent of approximately 100 km produce most of the depleted continental root. The upwellings in the large-scale time-dependent convection pattern below the depleted zone are located where the events of melt production show horizontal alignments in Fig. 4b. The arrows in Fig. 4 point to a single event which we have isolated for a more detailed investigation. This event is representative for the other episodic occurrences of partial melting.

Fig. 5a1–d1 shows a time sequence of blow-up snapshots of the degree of depletion together with flow patterns indicated by the contours of the instantaneous stream-function field. The corresponding modified temperature fields are given in Fig. 5a2–d2 together with several selected isotherms defined in

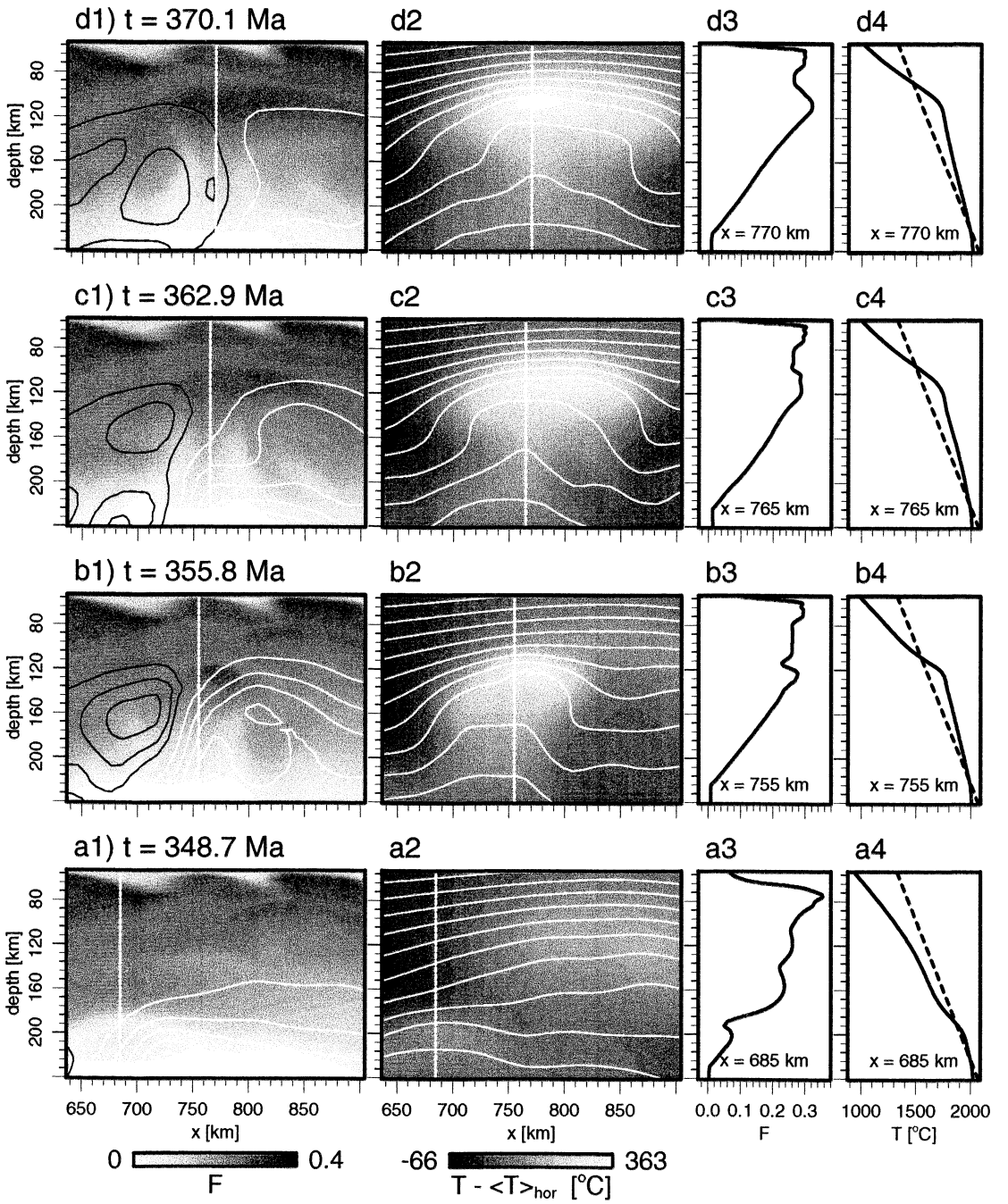

Fig. 5. Evolution in time of the event indicated with black arrows in Fig. 4 displayed in more detail. Streamlines in (a1–d1) are selected contours of the instantaneous stream function: white and black lines indicate clockwise and counterclockwise flow, respectively. The white isotherms in (a2–d2) have an increment of 110ºC and put the grey tone contours of the modified temperature field into perspective. (a3–d3) Shows vertical cross-sections of the degree of depletion through the centre of the diapir at the *x*-coordinate shown in each figure. The cross-section locations are also shown as white vertical dashed lines in the contour plots. (a4–d4) Shows cross-sections of the temperature at the same locations together with the solidus for undepleted material (dashed).

the figure caption. At the bottom of Fig. 5a1 a small diapir with a low degree of partial melting appears at a depth at about 210 km at $x = 685$ km. This small feature originates from the undepleted mantle and collides with the depleted layer. Vertical profiles through the centre and the tail of this diapiric upwelling are given in Fig. 5a3 and Fig. 5a4 for F and T, respectively, at the x-coordinate printed in the figure and indicated by the dashed vertical white line in the first two columns. The compositional buoyancy which increases due to melting in the head of the diapir facilitates the penetration into the continental root (compare Fig. 5a1–a4 with Fig. 5b1–b4). After a fast initial ascend the diapir becomes stagnant (compare Fig. 5b1–b4 and Fig. 5c1–c4). This stagnation is a combined effect of the increased viscosity of the MBL at shallower depth and the decrease in degree of depletion contrast of the diapir with its environment. The high-temperature feature in the upper right corner of Fig. 5a2 is the remnant of an older diapir which stagnated in this position as described above.

In the temperature profiles of Fig. 5a2–d2 the location of maximum deviation from the (dashed) solidus can be seen to move upward with the diapiric head, illustrating the ongoing melt production during the ascent and after stagnation. Note that the diapiric head produces a mushroom-shaped thin depleted layer at a depth of approximately 100 km (Fig. 5d1,d3) and that the tail of the diapir has also been subject to partial melting resulting in an almost linear vertical depletion profile (b3–d3).

Internal circulation of differentiated material within the depleted zone does not generate new melt in significant amounts. This is because in order to allow recurrent melting, the super-solidus temperature of mantle material (defined in the Appendix A) must be brought to a higher value than the maximum value it has experienced previously. This process of recurrent melting does not seem to be significant in a depleted zone subject to secular cooling. This means that the growth of the continental root in our model takes place almost exclusively through the growth of the depleted zone by the addition of depleted material derived from upwelling fertile material in the slowly convecting layer beneath the depleted zone. This process takes place in an episodical way as illustrated in Figs. 4 and 5.

3.7. Effects of F-dependent rheology

Model B is characterized by a rheology which depends on the degree of depletion through the viscosity pre-factor $\mathcal{B}(F)$. Time series of global-averaged quantities for this model are shown as dashed lines in Fig. 2. At about 200 Ma a downwelling of depleted material develops at the vertical boundary causing an upward return flow which generates the sudden increase in the volume-averaged value of the degree of depletion shown in Fig. 2c. The higher viscosity of the depleted material decreases its mobility and the convective heat transport through the layer. As a result the volume-averaged temperature shown in Fig. 2b is slightly higher than in Model A. This reduced cooling rate of Model B does not influence the principle growth process of the continental root.

The overall characteristics of this model differ only slightly from Model A where the rheology is independent of the degree of depletion F. No onset of continental delamination was observed in the 1 Ga time window of the model calculations. It can be expected that this onset will be delayed with respect to Model A due to the higher viscosity of the depleted zone and the related reduced rate of secular cooling.

4. Discussion

The modelling results show that a compositionally layered structure rapidly develops that will remain stable over long periods of time. After sufficiently long time, however, secular cooling results in gravitational instability and continental delamination. In Model A delamination sets in after a period of time t_d about 1.5 Ga. The value of t_d is related to several approximations made in the model. The zero heat flux condition applied at the depth of 670 km results in a secular cooling rate which is too high. Furthermore, the solidus temperature in the simplified melting phase diagram used overestimates the real solidus temperature to an increasing extent for increasing depth or pressure. This results in an underestimated amount and duration of the mantle differentiation. In future work we plan to improve our model in order to eliminate these limitations and obtain more realistic evolution time scales for the continental upper mantle.

Most observational evidence on the thickness of old continental roots comes from seismology and this evidence can be compared with our findings. In Fig. 3d a compositionally distinct root up to 200 km is shown which is in reasonable agreement with the depth of the drop in the seismic shear velocity between 170 and 200 km given by Anderson (1990). According to some authors (Jordan, 1988; Polet and Anderson, 1995) the compositional layer that forms the continental root may be thicker. We expect that such depths larger than 200 km of the root will occur in our model when a more accurate solidus and liquidus parameterization is applied (Takahashi, 1990; Vlaar et al., 1994).

The continental root growth mechanism in our model is an episodical diapiric process which results in a small-scale shallow layering (see Fig. 3e) which might explain seismic reflections from the shallow part of the continental upper mantle below the Moho discontinuity. These reflections could be associated with the remnants of mantle melting events (Flack and Warner, 1990). Melt segregation to a higher level or melt trapped in the mushroom-shaped diapiric heads can form layers which may act as good reflectors. Best (1991) describes such a reflecting zone at approximately 72 km depth beneath the Archaean terrain of the Montana Great Plains. The highlighted diapir in Fig. 5 reaches a depth of near 100 km (Fig. 5d3), which suggests that these seismic reflections may be related to such an ancient event.

The size of the diapiric events appear to be small compared to events responsible for the generation of outbursts of flood basalts. The diapir highlighted in Figs. 4 and 5 is one of the greater occurrences of melt generation and the amount of melt that is generated by this upwelling feature was estimated at 170,000 km^3. This estimate is based on the assumption that the width in the x-direction equals the width perpendicular to the 2-D model. Volume estimates of the smaller flood basalts start at approximately 750,000 km^3 and the generated volumes for the larger outflows are estimated at several millions of cubic kilometres (White and McKenzie, 1989; Farnetani and Richards, 1994).

A more quantitative comparison of the studied models can be made through the observed surface heat flow data. Heat loss through the top of the crust decreases from approximately 130 mW m^{-2} during the early stages for Model A, to approximately 100 mW m^{-2} after 1 Ga evolution. These are reasonable values since they are consistent with observational data. A present-day value for old cratons is about 50 mW m^{-2} and 80 ± 20 mW m^{-2} for younger continental shields (Vitorello and Pollack, 1980; Chapman, 1986; Pollack et al., 1993). The present model results are best compared to the heat flow data for younger continental crust, which have not been subject to secular cooling as long as the present-day Archaean shields. The values found from the models do not have any contribution from the lower mantle. Hence, the heat flow values found are lower bounds.

Finally, a restriction of the presented models is that they incorporate an isolated continental environment. Therefore, extrapolation of the thermal evolution from the present models to the whole Earth is not straightforward, since oceanic evolution is known to have different characteristics. Influence of ocean–continent interactions at shallow and deep levels are thus excluded from the present discussion.

5. Conclusions

The results of our modelling experiments have shown that stable continental structures with a compositional root can exist over long periods of time (>1.5 Ga). This long-term stability results from the density gradient related to the degree of depletion in the continental root. Also the temperature- and pressure-dependent rheology is important in preventing the continental root from collapse during secular cooling.

Potential temperatures in the model of the Archaean continental mantle were found to be in the range of $1700 < T_{pot} < 1900$ºC. These values proved to be sensitive to characteristics of the layering, in particular to the rheology of the depleted zone.

The continental growth process is an essential ingredient for continental lithospheric stability. In fact, stability comes to an end in our model when cooling from the top has brought the averaged geotherm below the peridotite solidus and mantle differentiation by partial melting stops. The evolution time scale $t_d = 1.5$ Ga found from or models, corresponding to the onset of continental delamination should be considered as a lower bound for the following rea-

sons. Firstly, the thermal coupling between the upper and lower mantle has been neglected in the model resulting in an overestimation of the secular cooling. Secondly, the parameterization of the melting phase diagram uses simple linearized versions of the solidus and liquidus of mantle peridotite. This in turn minimizes the amount of melt produced and the duration of melt production during secular cooling. A more realistic parameterization of the solidus and liquidus will result in melting in a wider depth range and over a longer time period during secular cooling. This in turn would result in a thicker and further differentiated continental root, which would extend to greater depths. This is in line with depths of 300 km found in Jordan (1988) and Polet and Anderson (1995).

Acknowledgements

This research was partly supported by NCF and NATO and partly carried out during a visit of Jeroen de Smet at the Minnesota Supercomputer Institute. Support was also received from the Netherlands Geosciences Foundation (GOA) with financial aid from the Netherlands Organisation for Scientific Research (NWO) through hard-ware grant NWO-750.396.02. We thank David Yuen for helpful discussions. Yannick Ricard and an anonymous reviewer are thanked for their helpful comments which improved the manuscript.

Appendix A

The differential of the degree of depletion $\mathrm{d}F$ can be expressed in terms of the solidus and liquidus temperatures T_s and T_l, and a melting curve $f(\Theta)$ in terms of the 'super-solidus temperature' Θ. We relate F and f through:

$$F(p,T) = f\left(\frac{T - T_\mathrm{s}(p)}{T_\mathrm{l}(p) - T_\mathrm{s}(p)}\right) = f\left(\frac{T - T_\mathrm{s}(p)}{\Delta T_\mathrm{sl}(p)}\right) = f(\Theta) \tag{6}$$

where T is the dimensioned temperature and Θ is the normalized 'super-solidus temperature', with $0 \leq \Theta \leq 1$, i.e. in between solidus and liquidus. The differential $\mathrm{d}F$ is given by:

$$\mathrm{d}F = \frac{\partial F}{\partial p}\mathrm{d}p + \frac{\partial F}{\partial T}\mathrm{d}T \tag{7}$$

where the partial derivatives are defined as:

$$A = \frac{\partial F}{\partial p} = \frac{\mathrm{d}f}{\mathrm{d}\Theta}\frac{\partial \Theta}{\partial p} = \frac{\mathrm{d}f}{\mathrm{d}\Theta}\left[-\Delta T_\mathrm{sl}^{-1}\frac{\mathrm{d}T_\mathrm{s}}{\mathrm{d}p} - (T - T_\mathrm{s})\Delta T_\mathrm{sl}^{-2}\frac{\mathrm{d}}{\mathrm{d}p}\Delta T_\mathrm{sl}\right] \tag{8}$$

$$B = \frac{\partial F}{\partial T} = \frac{\mathrm{d}f}{\mathrm{d}\Theta}\frac{\partial \Theta}{\partial T} = \Delta T_\mathrm{sl}^{-1}\frac{\mathrm{d}f}{\mathrm{d}\Theta} \tag{9}$$

In Eqs. 8 and 9 the slope of the phase equilibrium lines $\mathrm{d}T_\mathrm{s}/\mathrm{d}p$ is treated as a known constant material property.

In the present model we have used parallel, linear solidus and liquidus curves, i.e. $\mathrm{d}\Delta T_\mathrm{sl}/\mathrm{d}p = 0$. Furthermore, $\mathrm{d}T_\mathrm{s}/\mathrm{d}p = 120$ nK Pa^{-1} is a constant taken from Takahashi and Kushiro (1983) and $T_\mathrm{s}(p=0) = 1115$°C. We have used a linearized parameterization of the super-solidus melting curve of Jacques and Green (1980) with constant $\mathrm{d}f/\mathrm{d}\Theta = 1$. This parameterization results in constant values of the coefficients $A = -2 \times 10^{-10}$ Pa^{-1} and $B = \frac{1}{600}$ K^{-1}.

Recurrent melting in recycled depleted material will only take place if the volume is subject to super-solidus temperatures that exceeds any previously experienced.

References

Anderson, D.L., 1990. Geophysics of the continental mantle: a historical perspective. In: Menzies, M. (Ed.), Continental Mantle. Clarendon Press, Oxford, pp. 1–30.

Best, J.A., 1991. Mantle reflections beneath the Montana Great Plains on consortium for continental reflection profiling seismic reflection data. J. Geophys. Res. 96, 4279–4288.

Chapman, D.S., 1986. Thermal gradients in the continental crust. In: Dawson, J.B., Carswell, D.A., Hall, J., Wedepohl, K.H. (Eds.), The Nature of the Lower Continental Crust. Geol. Soc. London Spec. Publ. 24, 63–70.

Doin, M.-P., Fleitout, L., Christensen, U., 1997. Mantle convection and stability of depleted and undepleted continental lithosphere. J. Geophys. Res. 102, 2771–2787.

Doin, M.-P., Fleitout, L., McKenzie, D., 1996. Geoid anomalies and structure of continental and oceanic lithospheres. J. Geophys. Res. 101, 16119–16135.

Farnetani, C.G., Richards, M.A., 1994. Numerical investigations of the mantle plume initiation model for flood basalt events. J. Geophys. Res. 99, 13813–13833.

Flack, C., Warner, M., 1990. Three-dimensional mapping of seismic reflections from crust and upper mantle, northwest of Scotland. Tectonophysics 173, 469–481.

Hughes, T.J.R., Brooks, A., 1979. A multidimensional upwind scheme with no crosswind diffusion. In: Hughes, T.J.R. (Ed.), Finite Element Methods for Convection Dominated Flows. Applied Mechanics Division Vol. 34, ASME, New York.

Ita, J., King, S.D., 1994. Sensitivity of convection with endothermic phase change to the form of governing equations, boundary conditions and equation of state. J. Geophys. Res. 99, 15919–15938.

Jacques, A.L., Green, D.H., 1980. Anhydrous melting of peridotite at 0–15 kb pressure and genesis of tholeiitic basalts. Contrib. Mineral. Petrol. 73, 287–310.

Jordan, T.H., 1975. The continental tectosphere. Rev. Geophys. Space Phys. 13, 1–12.

Jordan, T.H., 1978. Composition and development of the continental tectosphere. Nature 274, 544–548.

Jordan, T.H., 1979. Mineralogies, densities, and seismic velocities of garnet lherzolites and their geophysical implications In: Boyd, F.R., Meyer, H.O.A. (Eds.), The Mantle Sample: Inclusions in Kimberlites and Other Volcanics. American Geophysical Union, Washington, DC, pp. 1–14.

Jordan, T.H., 1988. Structure and formation of the continental tectosphere. J. Petrol. Spec. Lithosphere Iss., 11–37.

Karato, S., Wu, P., 1993. Rheology of the upper mantle: a synthesis. Science 260, 771–778.

Lambeck, K., Johnston, P., Smither, C., Nakada, M., 1996. Glacial rebound of the British Isles, iii. Constraints on mantle viscosity. Geophys. J. Int. 125, 340–354.

Lenardic, A., 1997. On the heat flow variation from Archean cratons to Proterozoic mobile belts. J. Geophys. Res. 102, 709–721.

McKenzie, D., 1984. The generation and compaction of partially molten rock. J. Geophys. 25, 713–765.

O'Connell, R.J., Hager, B.H., 1980. On the thermal state of the Earth. In: Dziewonski, A.M., Boschi, E. (Eds.), Physics of the Earth's Interior. Elsevier, New York, pp. 270–317.

Ogawa, M., 1988. Numerical experiments on coupled magmatism–mantle convection system: implications for mantle evolution and Archean continental crusts. J. Geophys. Res. 93, 15119–15134.

Ogawa, M., 1993. A numerical model of a coupled magmatism–mantle convection system in Venus and the Earth's mantle beneath Archean continental crusts. Icarus 102, 40–61.

Ogawa, M., 1994. Effects of chemical fractionation of heat-producing elements on mantle evolution inferred from a numerical model of coupled magmatism–mantle convection system. Phys. Earth Planet. Inter. 83, 101–127.

Pari, G., Peltier, W.R., 1996. The free-air gravity constraint on subcontinental mantle dynamics. J. Geophys. Res. 101, 28105–28132.

Polet, J., Anderson, D.L., 1995. Depth extent of cratons as inferred from tomographic studies. Geology 23, 205–208.

Pollack, H.N., Hurter, S.J., Johnson, J.R., 1993. Heat flow from the Earth's interior: analysis of the global data set. Rev. Geophys. 31, 267–280.

Ranalli, G., 1991. The microphysical approach to mantle rheology. In: Sabadini, R., Lambeck, K., Boschi, E. (Eds.), Glacial Isostasy, Sea-Level and Mantle Rheology. Kluwer, Dordrecht, pp. 343–378.

Ringwood, A.E., 1982. Phase transformations and differentiation in subducted lithosphere: implications for mantle dynamics, basalt petrogenesis, and crustal evolution. J. Geol. 90, 611–643.

Schmeling, H., Bussod, G.Y., 1996. Variable viscosity convection and partial melting in the continental asthenosphere. J. Geophys. Res. 101, 5411–5423.

Segal, A., 1982. Aspects of numerical methods for elliptic singular perturbation problems. SIAM J. Sci. Stat. Comput. 3, 327–349.

Sotin, C., Parmentier, E.M., 1989. Dynamical consequences of compositional and thermal density stratification beneath spreading centers. Geophys. Res. Lett. 16, 835–838.

Sparks, D.W., Parmentier, E.M., 1993. The structure of three-dimensional convection beneath oceanic spreading centers. Geophys. J. Int. 112, 81–91.

Steinbach, V., 1991. Numerische Experimente zur Konvektion in kompressiblen Medien. Ph.D. thesis, Mitteilungen aus dem Institut für Geophysik und Meteorologie der Univ. zu Koeln 79.

Takahashi, E., 1990. Speculations on the Archean mantle: missing link between komatiite and depleted garnet peridotite. J. Geophys. Res. 95, 15941–15954.

Takahashi, E., Kushiro, I., 1983. Melting of a dry peridotite at high pressure and basalt magma genesis. Am. Mineral. 68, 859–879.

Ten, A., Yuen, D.A., Larsen, T.B., Malevsky, A.V., 1996. The evolution of material surfaces in convection with variable viscosity as monitored by a characteristics-based method. Geophys. Res. Lett. 23, 2001–2004.

Turcotte, D.L., Schubert, G., 1982. Geodynamics; Applications of Continuum Physics to Geological Problems. Wiley, New York.

Van den Berg, A.P., van Keken, P.E., Yuen, D.A., 1993. The effects of a composite non-Newtonian and Newtonian rheology on mantle convection. Geophys. J. Int. 115, 62–78.

Vitorello, I., Pollack, H.N., 1980. On the variation of continental heat flow with age and the thermal evolution of continents. J. Geophys. Res. 85, 983–995.

Vlaar, N.J., van den Berg, A.P., 1991. Continental evolution and Archaeo-sea-level. In: Sabadini, R., Lambeck, K., Boschi, E. (Eds.), Glacial Isostasy, Sea-Level and Mantle Rheology. Kluwer, Dordrecht, pp. 637–662.

Vlaar, N.J., van Keken, P.E., van den Berg, A.P., 1994. Cooling of the earth in the Archaean; consequences of pressure-release melting in a hotter mantle. Earth Planet. Sci. Lett. 121, 1–18.

White, R., McKenzie, D., 1989. Magmatism at rift zones: the generation of volcanic continental margins and flood basalts. J. Geophys. Res. 94, 7685–7729.